A Dual-Band MIMO Antenna System for 2.4/5 GHz WLAN Applications

Weiquan Zhang, Yue Li, *Senior Member, IEEE*, Kunpeng Wei, *Senior Member, IEEE*, and Zhijun Zhang, *Fellow, IEEE*

***Abstract*— A compact multiple-input-multiple-output (MIMO) microstrip antenna system covering the 2.4 and 5 GHz wireless local area network (WLAN) bands is presented in this article. To achieve dual-band characteristics, the TM_{01} and TM_{03} modes of a microstrip antenna are excited. A rectangular slot is etched in the center of the microstrip antenna for improving the radiation capability of the TM_{03} mode. Then, two probes are utilized to tune the resonant frequency of the TM_{01} mode with limited effect on the operating frequency of the TM_{03} mode. To realize high interport isolation at the two distinct WLAN bands in a methodological way, isolation enhancement is achieved successively at the lower and upper-frequency bands. Two split loops are introduced to reduce the mutual coupling at the 2.4 GHz band. Two dipole elements are added in the rectangular slot to obtain high isolation at the 5 GHz band. The decoupling mechanism of the proposed antenna is detailed analyzed. The proposed antenna system operates at 2.25–2.63 and at 5.14–6.06 GHz. The measured maximum value of mutual coupling between the two ports is less than −15.3 dB at both operating frequency bands.**

***Index Terms*— Antenna decoupling, dual-band antenna, microstrip antenna, multiple-input-multiple-output (MIMO) antenna.**

I. Introduction

HIGH data rate is desired for wireless communication to accommodate increasing wireless services. Multiple-input-multiple-output (MIMO) technology has gained much attention for its unique properties in terms of increasing channel capacity and improving reliability [1]. To realize an MIMO antenna system, multiple antennas are placed in a certain area. Consequently, signal interference occurs among antennas, especially when space is limited [2], [3], [4]. Hence, it is a challenge to decouple compactly placed multiple antennas in an MIMO system. Many compact single-band WLAN antennas have been studied [5], [6], [7]. However, multiband antennas are urgently required due to the rapid growth of wireless services. For instance, the wireless local area network (WLAN) standard IEEE 802. 11ax covers the 2.4 and 5 GHz bands. Therefore, a dual-band antenna simultaneously covers the two distinct bands is desired. How to achieve high isolation between multiband antenna elements becomes a critical issue for an MIMO WLAN system.

There are many works focusing on the port decoupling of single-band MIMO antenna systems [8], [9], [10], [11], [12], [13]. Defected ground structure (DGS) [8], [9], metasurface [10], neutralization line [11], and parasitic resonator [12] loading are common methods to realize mutual coupling reduction. These methods have also been utilized for multiband antenna decoupling. In general, by etching DGS (slot/slit) on the ground between/around the antennas, the mutual coupling between ports can be reduced [14], [15], [16]. In [16], by respectively introducing two slots on each side of the antenna, high isolation was achieved at the 2.4 and 5 GHz bands but with a high profile of 10 mm. In general, the DGS requires additional space, resulting in the uncompacted size of the antenna. Besides, the ground plane is desired to be intact in many practical scenarios. Dual-band decoupling can also be realized by placing the metasurface between or above the antennas [17], [18], [19], [20]. In [17], a modified array antenna decoupling surface was designed and placed above a microstrip antenna system for improving the isolation at the lower band but with a high profile. A low profile can be obtained by placing decoupling metasurface between the antennas [19], [20]. The introduction of metasurface will undoubtedly increase the size and complexity of the antenna system. In [21], the neutralization technique was utilized to decouple a dual-band antenna array. Introducing parasitic resonators on/around/between the antennas is also an effective method to achieve multiband decoupling [22], [23], [24], [25]. The authors presented a wideband loop resonator for isolation enhancement in dual-band microstrip antenna arrays [22]. Besides, decoupling networks have been widely studied for multiband antenna decoupling [26], [27], [28], [29], [30]. Decoupling networks have good generality but with insertion loss and complex optimization processes. In this work, an effort is put to develop a compact dual-band two-element antenna system with high isolation at two different bands.

Manuscript received 5 January 2023; revised 23 April 2023; accepted 24 April 2023. Date of publication 22 May 2023; date of current version 7 July 2023. This work was supported by the National Natural Science Foundation of China under Contract 61971254 and Contract 62271279. *(Corresponding author: Zhijun Zhang.)*

Weiquan Zhang, Yue Li, and Zhijun Zhang are with the Department of Electronic Engineering, and the Beijing National Research Center for Information Science and Technology, Tsinghua University, Beijing 100084, China (e-mail: zjzh@tsinghua.edu.cn).

Kunpeng Wei was with the Honor Device Company Ltd., Beijing 100095, China. He is now with the Xiaomi Communications Company Ltd., Beijing 100085, China, and also with the Department of Electronic Engineering, and the Beijing National Research Center for Information Science and Technology, Tsinghua University, Beijing 100084, China.

Color versions of one or more figures in this article are available at https://doi.org/10.1109/TAP.2023.3277208.

Digital Object Identifier 10.1109/TAP.2023.3277208

0018-926X © 2023 IEEE. Personal use is permitted, but republication/redistribution requires IEEE permission.
See https://www.ieee.org/publications/rights/index.html for more information.

Authorized licensed use limited to: Tsinghua University. Downloaded on December 18,2023 at 07:49:26 UTC from IEEE Xplore. Restrictions apply.

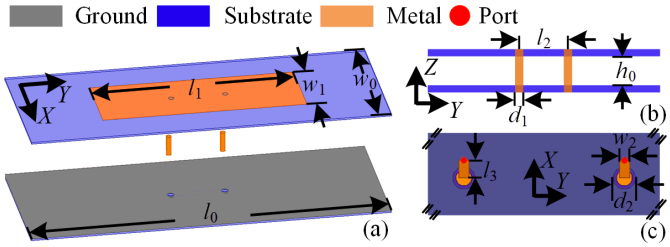

Fig. 1. Geometry of the microstrip antenna with two ports. (a) Layered, (b) side, and (c) rear views.

In this article, a dual-band MIMO microstrip antenna system is proposed for WLAN application. By exciting the TM_{01} and TM_{03} modes of a microstrip antenna, the proposed antenna operates at the 2.4 and 5 GHz bands. The resonant frequency of the TM_{01} mode can be independently tuned by two probes. The antenna decoupling is realized in an intuitive way. By introducing decoupling probes, split loops, and dipole elements, antenna decoupling is successively realized at the lower and upper bands. The designed dual-band MIMO antenna was implemented and tested. The proposed design is very compact and exhibits dual-band performance as well. which confirms that the proposed antenna can be a potential candidate for access point application.

The following contribution of the proposed antenna will be demonstrated:

1) A dual-band microstrip antenna is proposed and the evolution of the proposed antenna is given and discussed in detail.
2) The decoupling structures are integrated with the antenna without occupying extra space. Hence, the design is compact. Moreover, the decoupling structures are introduced in a methodological way.
3) The antenna decoupling is achieved at two Wi-Fi bands. The antenna decoupling at the upper band is independently realized.

The rest of this article is divided into four parts. In Section II, an overall description of the design of a dual-band microstrip antenna is given. Section III details the decoupling process of the antenna system. Section IV presents the simulated and measured results. Finally, a conclusion is given in Section V.

II. Antenna Design

Fig. 1 shows a microstrip antenna with two ports. The antenna contains two substrates, one metal plane, one ground plane, two probes, and two microstrip lines. The two probes connect the metal plane with the microstrip lines. The two 0.6 mm thick substrates are FR-4 of relative permittivity of 4.4 and loss tangent of 0.02. Detailed design parameters of the initial antenna are shown in Table I.

To simultaneously cover the 2.4 and 5 GHz bands, an intuitive way is to excite multiple modes of the microstrip antenna at the same time. The TM_{01} and TM_{03} modes are considered here owing to the appropriate operating frequency ratio of the two modes. The two modes have been studied and used to realize dual-band or wideband microstrip antennas [31], [32]. Fig. 2(a) shows the schematic

TABLE I
Detailed Dimension of the Antenna

Parameter	Value (mm)	Parameter	Value (mm)
l_0	120	w_1	25
l_1	68	w_2	1.15
l_2	18	d_1	1.8
l_3	2	d_2	2.5
w_0	50	h_0	5.4

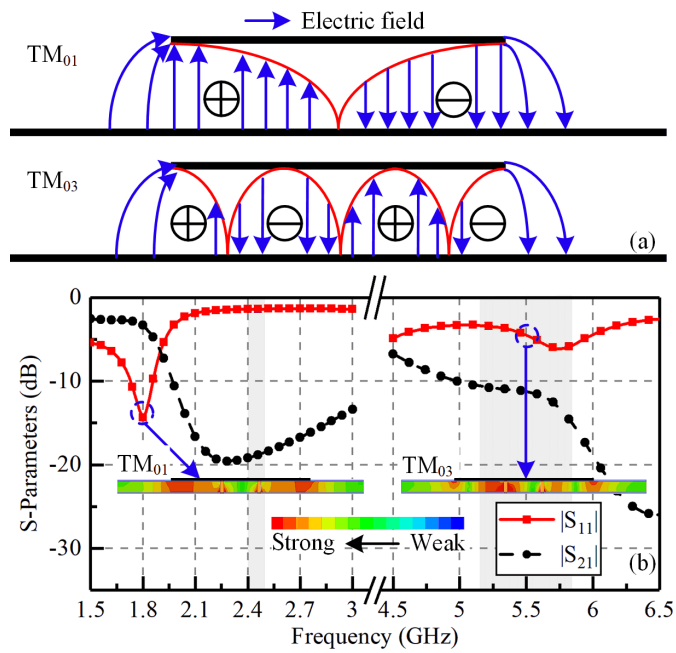

Fig. 2. (a) Schematic diagrams of the E-field intensity distributions for TM_{01} and TM_{03} modes. (b) Simulated S-parameters.

diagrams of E-field intensity distributions for TM_{01} and TM_{03} modes in the *YZ* plane. The electrical field distributions of TM_{01} and TM_{03} modes are sinusoidal and even-symmetric in the E-plane. As shown in Fig. 2(b), the TM_{01} and TM_{03} modes, respectively, operate around the 2.4 GHz band and at the 5 GHz band. Since the antenna is symmetrical in the *XZ* and *YZ* planes, the $|S_{22}|$ and $|S_{12}|$ results are not given for brevity.

The electric field at the radiating edge of the microstrip antenna can be equivalent to magnetic current. The two equivalent magnetic currents of the microstrip antenna have an electric distance larger than one wavelength within the 5 GHz band, resulting in a high sidelobe level. Besides, the wide operating bandwidth of the TM_{03} mode is desired to cover the wide 5 GHz band. To solve these two issues, a rectangular slot is etched in the center of the microstrip antenna, as shown in Fig. 3(a). Fig. 3(b) depicts the simulated E-field intensity distribution in the *YZ* plane at 5.5 GHz with port 1 excited. The electric field at the edge of the slot also radiates. Hence, the radiation aperture of TM_{03} mode is increased. Fig. 3(c) plots the simulated S-parameters of the microstrip antenna with rectangular slot etched. Better matching status is obtained at the 5 GHz band owing to the increased radiation aperture of TM_{03} mode. Fig. 4 depicts the simulated normalized co-

Authorized licensed use limited to: Tsinghua University. Downloaded on December 18,2023 at 07:49:26 UTC from IEEE Xplore. Restrictions apply.

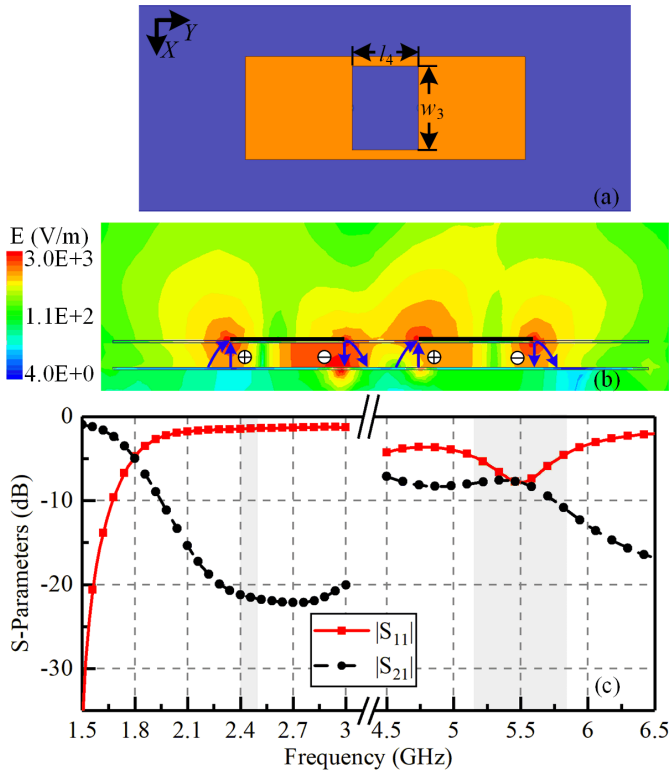

Fig. 3. (a) Top view of the microstrip antenna with a rectangular slot etched. (b) Simulated E-field intensity distribution at 5.5 GHz with port 1 excited. (c) Simulated S-parameters. Detailed dimensions: $l_4 = 16$ mm and $w_3 = 20.5$ mm.

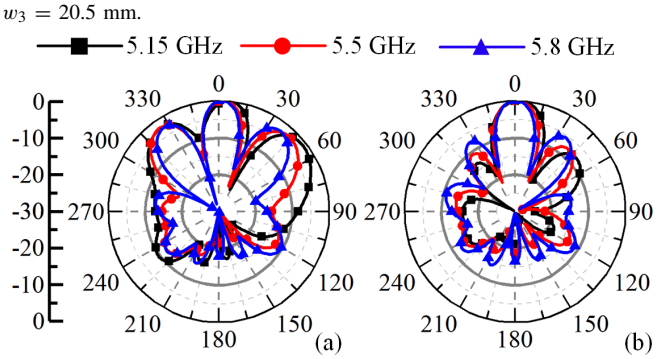

Fig. 4. Simulated normalized co-polarized radiation patterns in the *YZ* plane (a) without and (b) with the rectangular slot etched. The port 1 is excited and port 2 is connected to a 50 Ω load.

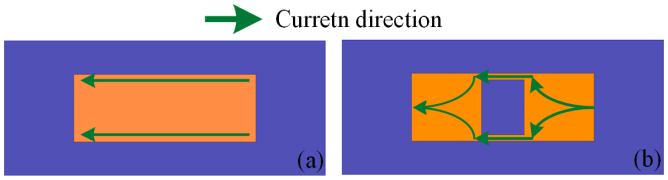

Fig. 5. Schematic diagrams of the current distributions for TM_{01} mode (a) without and (b) with the rectangular slot.

polarized radiation patterns without and with the rectangular slot etched. Sidelobe level reduction of 7, 5.7, and 3.2 dB is, respectively, achieved at 5.15, 5.5, and 5.8 GHz. The operating frequency of the TM_{01} mode moves to a lower frequency since the rectangular slot increases the current length of the TM_{01} mode, as shown in Fig. 5. The working frequency of the TM_{01} mode should be increased to cover the 2.4 GHz band. As shown in Fig. 2(a), the electric field intensity distributions

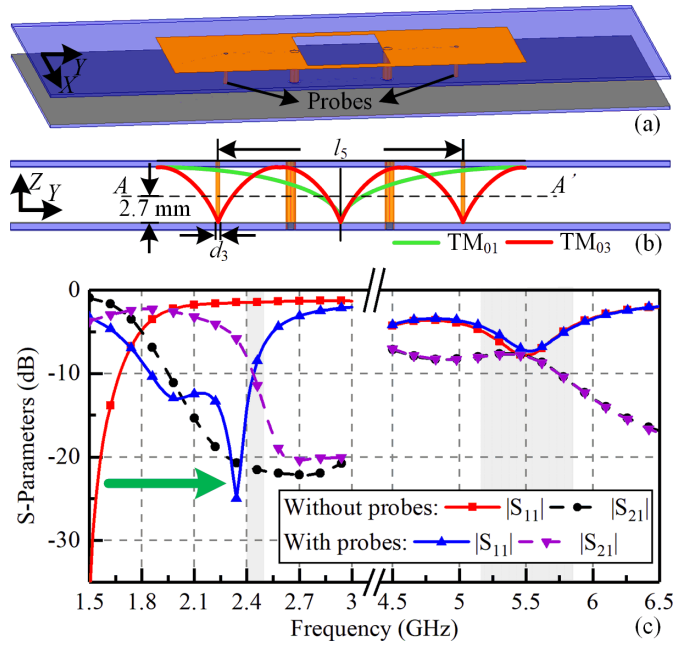

Fig. 6. (a) Perspective and (b) side views of the proposed antenna with two probes added. (c) Simulated S-parameters at the two distinct frequency bands. Detailed dimensions: $l_5 = 44.6$ mm and $d_3 = 0.8$ mm.

of the TM_{01} and TM_{03} modes are different, which can be utilized to adjust the resonant frequency of the TM_{01} mode with limited effect on the TM_{03} mode. As shown in Fig. 6(a), two probes are symmetrically added in the *YZ* plane. The two probes connect the metal ground with the metal plane. As shown in Fig. 6(b), the two probes are placed in the null points of electric field intensity for TM_{03} mode. Predictably, the effect of the two probes on the operating frequency of the TM_{03} mode is negligible. However, the electric field intensity distribution of the TM_{01} mode is affected by the two probes. The probe is equivalent to a parallel inductor, which increases the operating frequency of the TM_{01} mode. Fig. 6(c) plots the simulated S-parameters of the microstrip antenna with and without the two probes. By introducing the two probes, the operating frequency of the TM_{01} mode moves to around 2.44 GHz while the simulated S-parameters at the upper-frequency band are almost unchanged.

III. Antenna Decoupling

A dual-band microstrip antenna is realized in Section II. In this section, the interport isolation at the two distinct WLAN bands will be achieved based on the common mode (CM) and differential mode (DM) concepts [33], [34], [35]. For a symmetrical and reciprocal two-port antenna, the S_{11} and S_{21} can be described by the CM and DM S-parameters

$$S_{11} = S_{22} = \frac{S_{\mathrm{CM}} + S_{\mathrm{DM}}}{2}$$
$$S_{21} = S_{12} = \frac{S_{\mathrm{CM}} - S_{\mathrm{DM}}}{2}. \quad (1)$$

Antenna decoupling can be achieved with the same or similar CM and DM status, as shown in Fig. 7.

The DM and CM can be, respectively, obtained by exciting the two ports with out-of-phase and in-phase signals.

Authorized licensed use limited to: Tsinghua University. Downloaded on December 18,2023 at 07:49:26 UTC from IEEE Xplore. Restrictions apply.

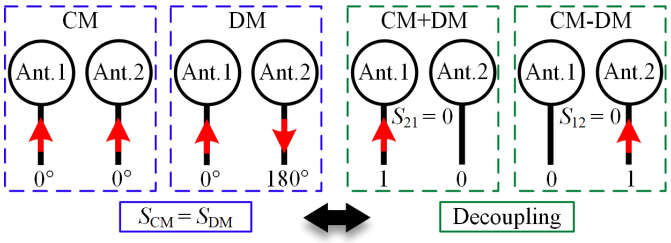

Fig. 7. Decoupling schematic diagrams based on the CM and DM cancellation.

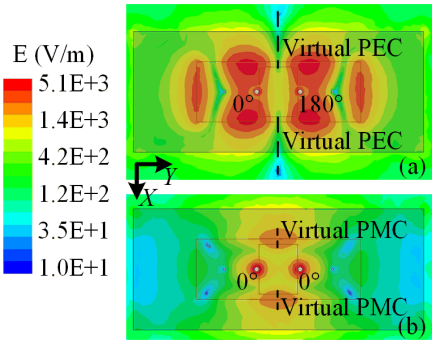

Fig. 8. Simulated electric field intensity distributions of the (a) DM and (b) CM in the XY plane containing the reference line AA' at 5.5 GHz.

The simulated S_{CM} and S_{DM} can be calculated based on the simulated S-parameters of the two ports. The antenna and the two ports are symmetrical in the XZ and YZ planes. As a result, when the DM and CM are excited, weak and strong electric field intensity distributions can be, respectively, observed under the middle of two metal strips, as shown in Fig. 8. Virtual perfect electric conductor (PEC) and perfect magnetic conductor (PMC) planes are, respectively, obtained with the DM and CM excited. This phenomenon can be observed in the two bands owing to the symmetrical characteristic of the antenna and feed ports. Therefore, two decoupling probes are introduced to independently tune the CM impedances at the two bands, as plotted in Fig. 9(a). As observed from Fig. 9(b) and (c), the CM impedances are adjusted by the two decoupling probes at the two frequency bands. However, the DM impedances remain almost constant. Fig. 9(d) depicts the simulated S-parameter with and without the two decoupling probes. The average interport isolation is about 10 and 8.5 dB at the lower and upper bands without the two decoupling probes. With the two decoupling probes added, the average interport isolation at the lower and upper bands is 11 and 14.8 dB, respectively. The isolation is significantly improved at the upper band since the CM and DM impedances are closer with the two decoupling probes added.

To mitigate the mutual coupling at the 2.4 GHz band, two metal strips were loaded on the bottom surface of the upper substrate, as shown in Fig. 10(a) and (b). The end of the strips is connected to the microstrip antenna through a metallic via. Fig. 10(c) depicts the simulated S-parameters with and without the metal strips. It can be seen that the isolation is improved to higher than 17.3 dB at the 2.4 GHz band with the two metal strips loaded. To further illustrate the decoupling mechanism, the decoupling structure was extracted and analyzed. The metal strip, metallic via, and part of the

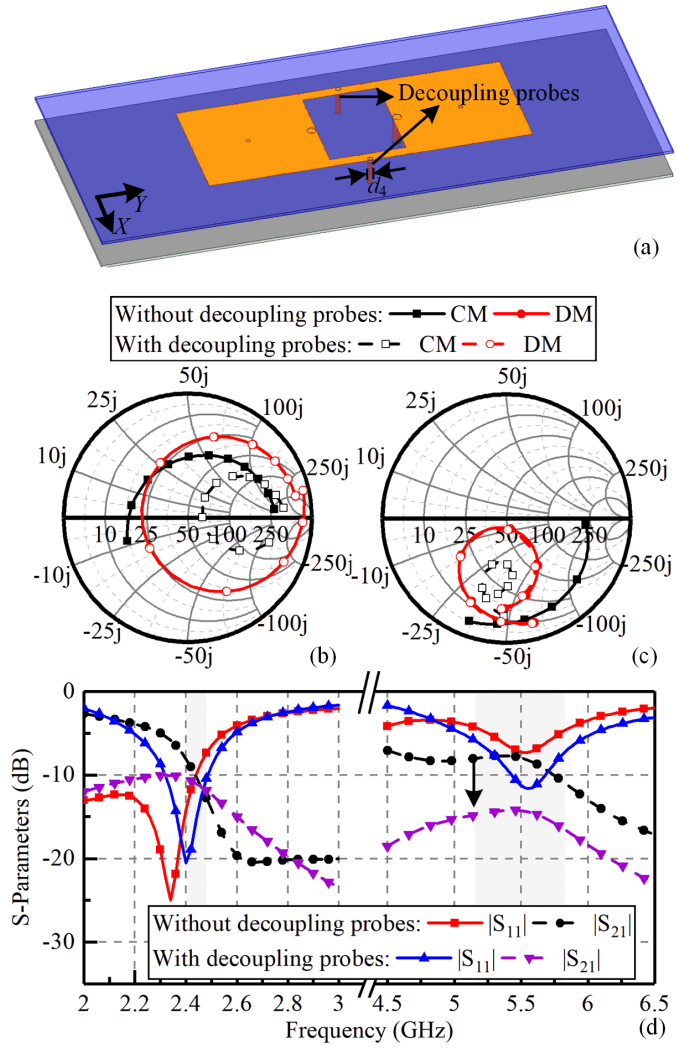

Fig. 9. (a) Proposed antenna with two decoupling probes added. Smith charts of the DM and CM impedances at (b) 2.4 and (c) 5 GHz frequency bands. (d) Simulated S-parameters without and with the decoupling probes. Detailed dimensions: $d_4 = 1$ mm.

microstrip antenna form a split loop. As shown in Fig. 11(a), a split loop model is extracted. The split loop will be excited by the microstrip antenna through energy coupling. The CM and DM status of the proposed antenna is considered here. So, two equivalent ports can be obtained with the same relative phase relationship of the two antenna ports. Fig. 11(b)–(d) plots the current distributions of the split loop under the DM and CM status.

Even and odd symmetry of the current direction along the central plane can be, respectively, observed under the CM and DM status. The working frequencies of resonant modes are related to the current length. Due to the loading of the substrate, the length of the split loop is about 1.5λ (λ is the equivalent wavelength at 2.44 GHz). Hence, the 3rd-order mode of the split loop may work at the 2.4 GHz band. As shown in Fig. 11(c), the DM status corresponds to the 3rd-order mode. Besides, the corresponding current distributions of the 2nd- and 4th-order modes are, respectively, depicted in Fig. 11(b) and (d). They can be excited under the antenna CM status but with different resonant frequencies. Compared to the 3rd-order mode (DM), the 2nd-order mode

Authorized licensed use limited to: Tsinghua University. Downloaded on December 18,2023 at 07:49:26 UTC from IEEE Xplore. Restrictions apply.

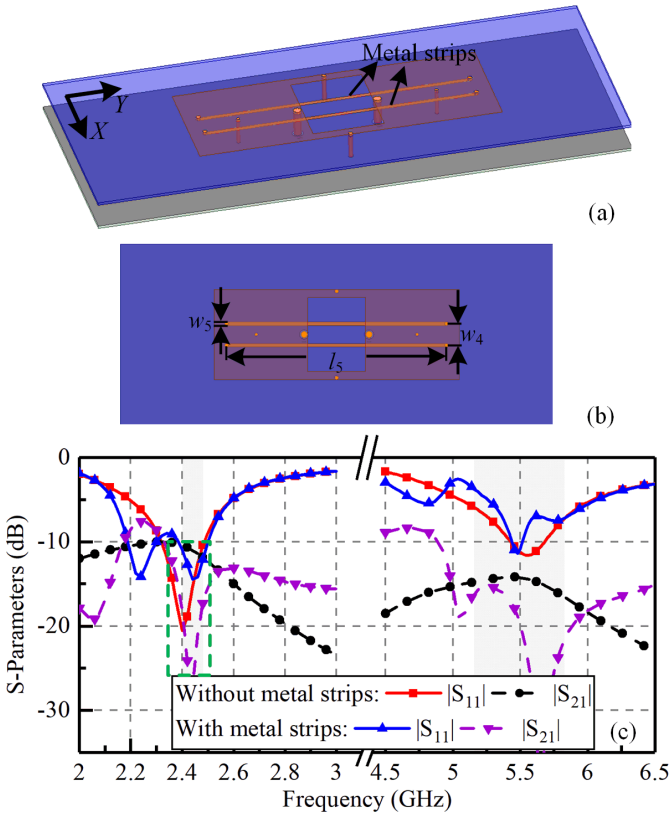

Fig. 10. (a) Perspective and (b) top views of the proposed antenna with two metal strips and two via loaded. (c) Simulated S-parameters. Detailed dimensions: $l_5 = 61$ mm, $w_4 = 6$ mm, and $w_5 = 1$ mm.

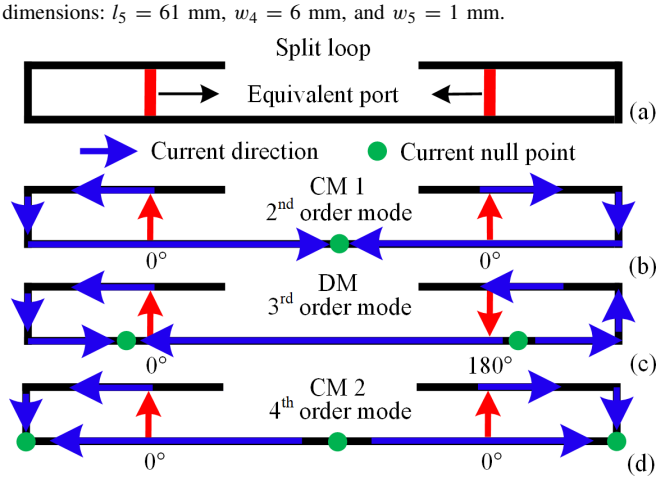

Fig. 11. (a) Schematic of the extracted split loop model. Current distributions of the split loop under (b) CM 1, (c) DM, and (d) CM 2 status.

(CM 1) operates at a lower frequency due to the longer current length. The 4th-order mode (CM 2) is reversed. Based on the current length and applied substrate, only the 3rd-order mode (DM) may work at/near the 2.4 GHz band. To verify the analysis, a simulation was taken. As shown in Fig. 12(a) and (b), a split loop with two lumped ports was considered with a 0.6 mm thick FR-4 substrate. Fig. 12(c) indicates that the CM impedances of the split loop are almost pure reactance at the 2.4 GHz band. So, the CM of the split loop cannot be effectively excited at the 2.4 GHz band. Fig. 12(d) plots the Smith chart of the microstrip antenna with and without the two split loops. By applying the two split

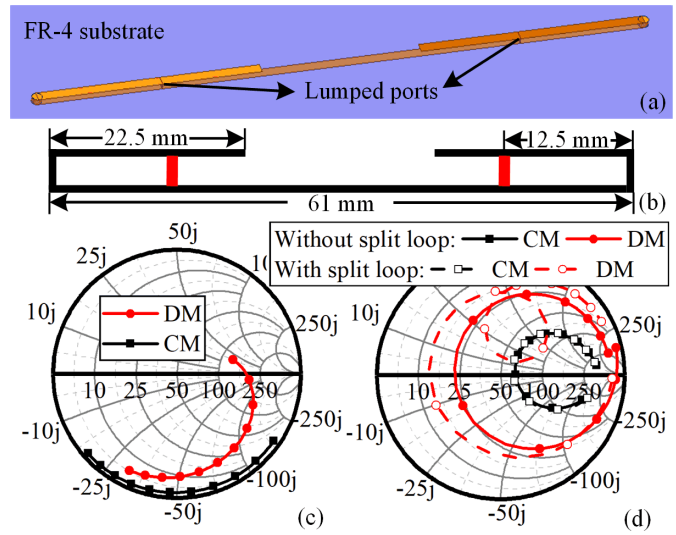

Fig. 12. (a) Simulated model of a split loop with two lumped ports. (b) Side view of the simulated model. Smith charts of the DM and CM impedances of (c) split loop and (d) proposed antenna at the 2.4 GHz frequency band.

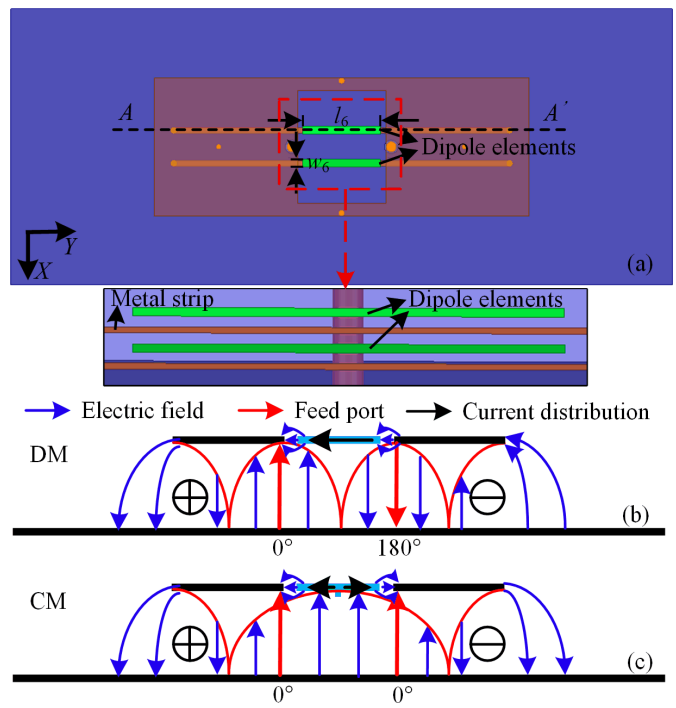

Fig. 13. (a) Top view of the proposed antenna with two dipole elements added. (b) Schematic diagrams of electric field intensity and current distributions in the YZ plane containing the reference line AA' for (b) DM and (c) CM status at the 5 GHz band. Detailed dimensions: $l_6 = 14$ mm and $w_6 = 1.4$ mm.

loops, the DM impedances of the antenna system are adjusted but with almost unchanged CM impedances at the 2.4 GHz band. Since the CM impedances of the split loop are almost pure reactance at the lower band, the split loop does not work under the antenna's CM status. Therefore, it has a limited impact on the CM status of the antenna. The CM and DM impedances of the microstrip antenna at the lower band are independently tuned by the decoupling probes and split loops, leading to high isolation at the lower band.

Authorized licensed use limited to: Tsinghua University. Downloaded on December 18,2023 at 07:49:26 UTC from IEEE Xplore. Restrictions apply.

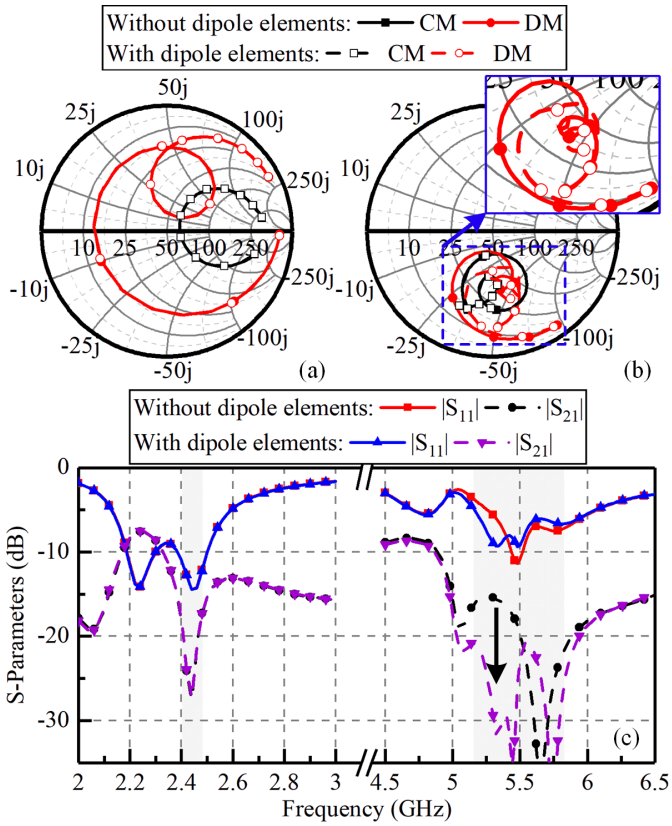

Fig. 14. Smith charts of the DM and CM impedances at the (a) 2.4 and (b) 5 GHz frequency bands. (c) Simulated S-parameters without and with dipole elements.

To further increase the isolation between the two ports at the 5 GHz band, two dipole elements are added in the rectangular slot, as shown in Fig. 13(a). To reveal the decoupling mechanism, the schematic diagrams of electric field intensity and current distributions at the 5 GHz band are depicted in Fig. 13(b) and (c). The dipole elements can be excited by the electric field at the edge of the rectangular slot. The 1st- and 2nd-order modes of the dipole elements can be excited under the DM and CM status, respectively. As we know, the 1st- and 2nd-order modes of a dipole antenna have different operating frequencies. Predictably, the distinct working frequencies of the two dipole modes can be utilized to independently tune the CM or DM impedances of the proposed antenna at a certain frequency band. The length of the dipole element is 14 mm, which is about half wavelength at 5.5 GHz with the FR-4 substrate loaded. Therefore, the dipole elements have the potential to independently adjust the DM impedances of the microstrip antenna at the 5 GHz band. Fig. 14(a) and (b), respectively, shows the Smith charts of the CM and DM impedances at the lower and upper bands. Because the electric length of the dipole element is much less than half wavelength at the 2.4 GHz band, it does not work at the lower band. As a result, the introduction of the dipole elements has an ignorable impact on the CM and DM impedances of the antenna at the 2.4 GHz band. The DM impedances are independently tuned at the 5 GHz band, as shown in Fig. 14(b). The simulated S-parameters of the proposed antenna with and without dipole elements are given in Fig. 14(c). The simulated S-parameter

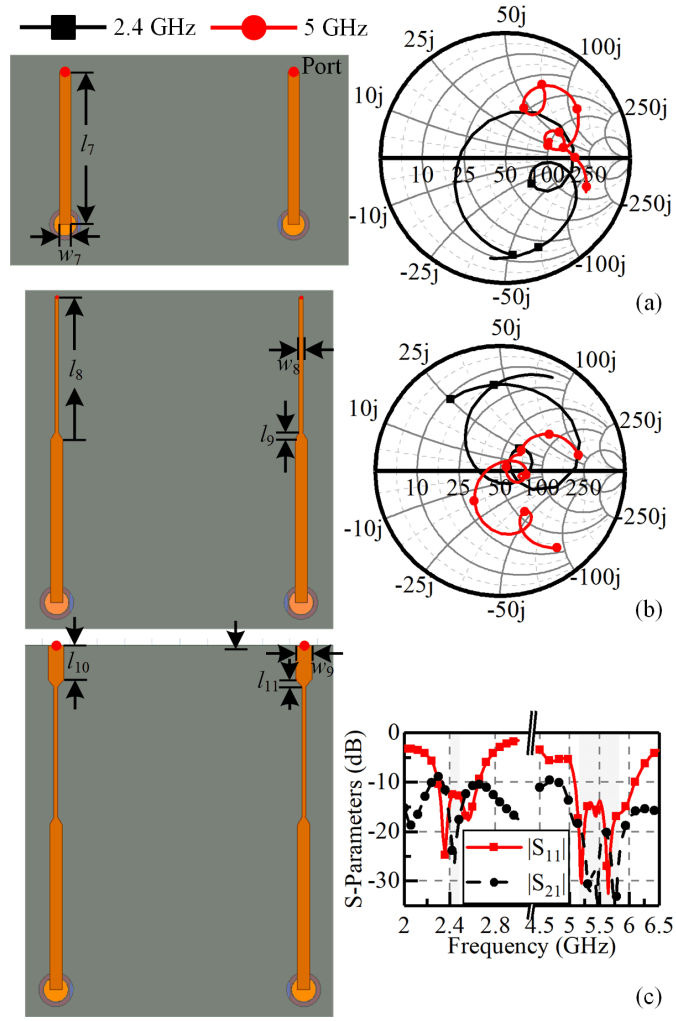

Fig. 15. Matching process of the proposed antenna at the two bands. (a) Status 1 and the corresponding Smith chart of Z_{11}. (b) Status 2 and the corresponding Smith chart of Z_{11}. (c) Status 3 and the corresponding simulated S-parameters. Detailed dimensions: $l_7 = 12$ mm, $l_8 = 10.5$ mm, $l_9 = 0.5$ mm, $l_{10} = 2.5$ mm, $l_{11} = 0.5$ mm, $w_7 = 0.9$ mm, $w_8 = 0.3$ mm, and $w_9 = 1.15$ mm.

at the lower band is almost unchanged. The interport isolation is improved to higher than 20 dB within the 5 GHz band with the dipole elements loaded. Hence, the mutual coupling reduction at the upper band is achieved without deteriorating the S-parameters at the lower band.

The port matching is realized using the microstrip lines. The matching evolutions of the antenna are given in Fig. 15. Microstrip lines with different characteristic impedances are utilized to adjust the matching status at the two bands. The characteristic impedance of the microstrip lines is changed by varying the width. As shown in Fig. 15(c), the two ports can cover the entire 2.4 and 5 GHz bands with $|S_{11}| > -10$ dB. The interport isolation is higher than 17.5 and 18.5 dB at the 2.4 and 5 GHz bands, respectively.

IV. Experimental Verification

To verify our proposal, a prototype of the proposed antenna was fabricated as shown in Fig. 16(a). The two substrates were fixed by four nylon posts. During the measurement, a 50 Ω SMA connector was utilized to feed one port of

Authorized licensed use limited to: Tsinghua University. Downloaded on December 18,2023 at 07:49:26 UTC from IEEE Xplore. Restrictions apply.

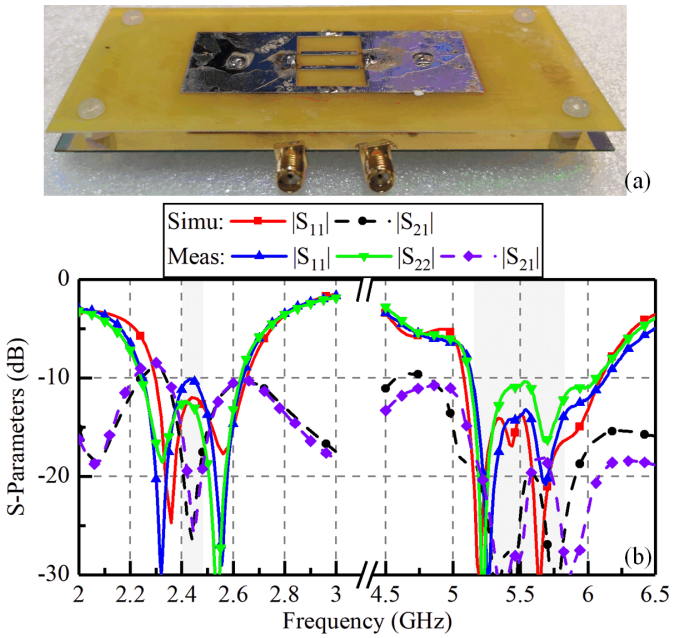

Fig. 16. (a) Photograph of the fabricated antenna. (c) Simulated and measured S-parameters.

the antenna. The other port was connected to a 50 Ω load. S-parameters of the antenna were measured using an N5071B vector network analyzer (300 kHz–9 GHz). The radiation performance of the proposed antenna was measured in a far-field anechoic chamber. It is demonstrated in Fig. 16 that the measured S-parameters agree well with the simulation. The results indicate that the proposed dual-band antenna operates at both the 2.4 and 5 GHz bands. The measured interport isolation is, respectively, higher than 15.3 and 17.6 dB at the lower and upper bands.

The simulated and measured normalized radiation patterns of the proposed dual-band antenna system at 2.4, 5.15, 5.55, and 5.8 GHz are shown in Fig. 17. One port was excited and the other one was connected to a 50 Ω load during the measurement. The simulated and measured results show agreement.

The envelope correlation coefficient (ECC) is an important figure of merit for benchmarking the performance of an MIMO system. The ECC for a two-element MIMO system can be calculated as

$$\rho_e = \frac{\left|\iint_{4\pi}\left[\vec{E_1}(\theta,\varphi)\cdot\vec{E_2}(\theta,\varphi)\right]d\Omega\right|^2}{\iint_{4\pi}\left|\vec{E_1}(\theta,\varphi)\right|^2 d\Omega \iint_{4\pi}\left|\vec{E_2}(\theta,\varphi)\right|^2 d\Omega} \tag{2}$$

where $E_i(\theta, \varphi)$ is the corresponding electric field radiated by the antenna with port i excited. The variation of ECC of the MIMO antenna with respect to frequency is shown in Fig. 18. The value of ECC at both operating bands is below 0.12.

Fig. 19 depicts the simulated and measured gains and efficiency of the antenna. The discrepancy between the simulated and measured results is acceptable considering the soldering and testing error. The measured average gain and total efficiency of the antenna are 5.2 dB and 81% at the 2.4 GHz band. An average gain of 6.7 dB and an average efficiency of 70.7% are obtained at the 5 GHz band.

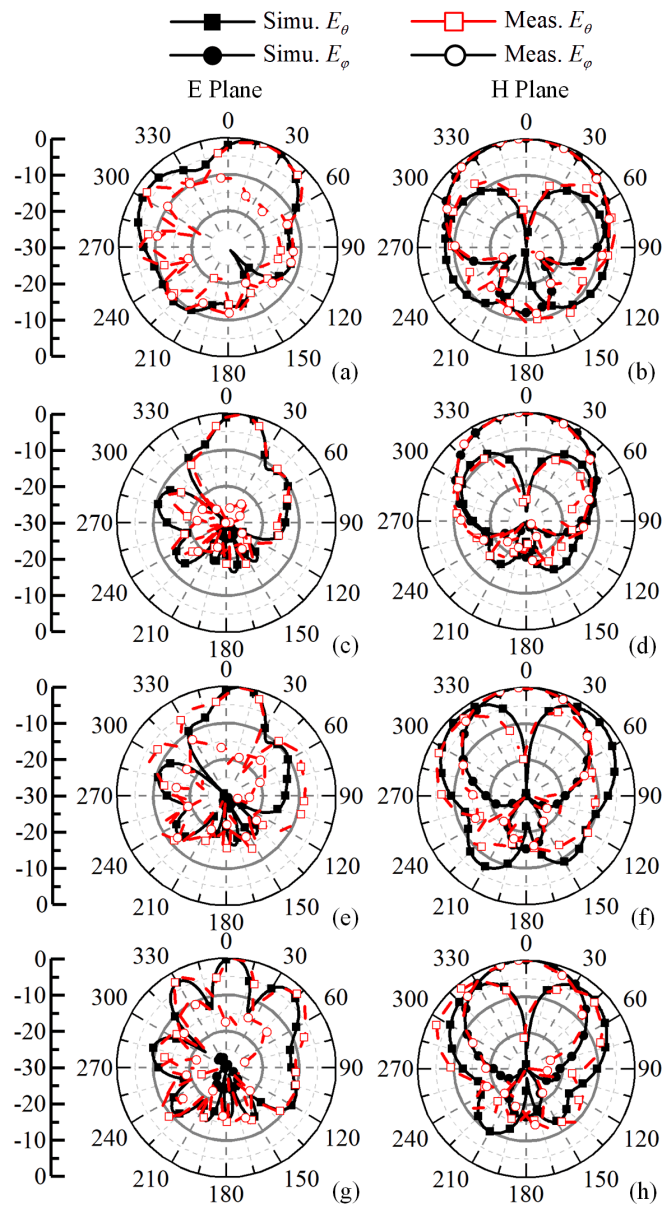

Fig. 17. Simulated and measured far-field patterns of the proposed antenna at (a) and (b) 2.4, (c) and (d) 5.15, (e) and (f) 5.55, and (g) and (h) 5.8 GHz with port 1 excited.

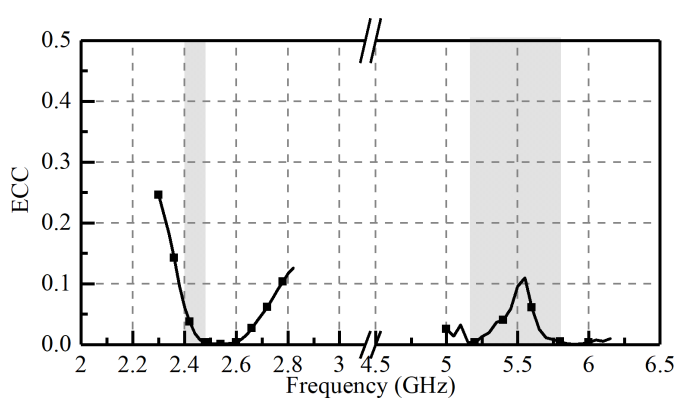

Fig. 18. Calculated ECC of the proposed antenna.

Authorized licensed use limited to: Tsinghua University. Downloaded on December 18,2023 at 07:49:26 UTC from IEEE Xplore. Restrictions apply.

TABLE II
COMPARISON AMONG THE RELEVANT WORKS

Ref.	Method	Frequency (GHz)	Bandwidth	Size (λ_L)	Edge to edge spacing (λ_0)	Isolation improvement (dB)	Side lobe level in E plane (dB)	HPBW in H plane (°)
[15]	DGS	2.4 - 2.67 / 5.46 - 5.73	10.7% / 4.5%	0.20×0.19× 0.01	0.03 / 0.07	8 → 20 / 17.5 → 22	∞ / ∞	> 90* / > 75*
[19]	EBG	3.42 - 3.6 / 4.7 - 5.1	5.1% / 8.2%	0.66×0.50× 0.01	0.46 / 0.65	15 → 40 / 15 → 25	> 3* / > 6*	Not given
[22]	Resonator	3.3 - 3.5* / 4.15 - 4.35*	5.9% / 4.7%	0.76×0.35× 0.02	0.057 / 0.07	12 → 27.1 / 9 → 25.3	∞ / ∞	> 90* / > 90*
[23]	Resonator	2.34 - 2.6/ 5.25 - 5.9	10.5% / 11.7%	0.35×0.30× 0.01	0.07 / 0.17	8.8 → 20.3 / 19.5 → 26.7	Not applicable	Not applicable
This Work	**Probe & resonator**	**2.25 - 2.63 / 5.14 – 6.06**	**15.6% / 16.4%**	**0.90×0.38× 0.05**	**Not applicable**	**9 → 15.3 / 8.5 → 17.6**	**> 3.3 / > 2.1**	**> 92 / > 59**

*: approximate values. λ_L: the free-space wavelength at the lowest working frequency.

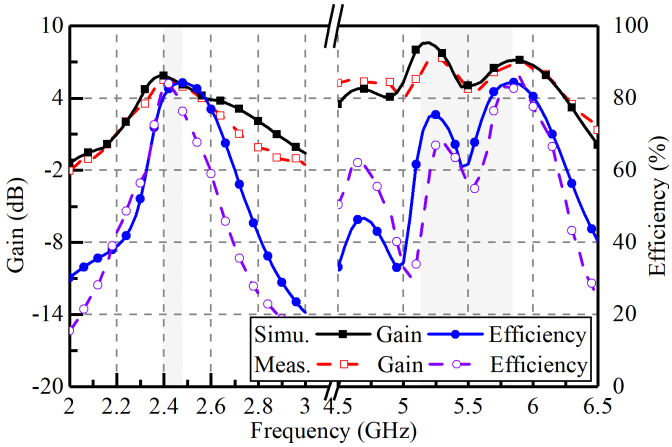

Fig. 19. Gains and efficiency of the proposed antenna.

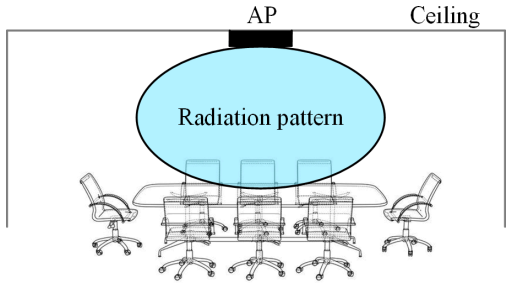

Fig. 20. Meeting room application scenario of the proposed antenna.

Table II summarizes the performance of this work and other relevant works. By applying the EBG, the antenna in [19] shows much better isolation enhancement at the cost of electrical size and complicated structure. The proposed decoupling structures are integrated with the antenna. Though the final achieved isolation is not very high, the original isolation at the two bands is also lower. Compared with other works, the widest operating bandwidth at the two bands is achieved in this work. Though a rectangular slot is applied in this work to reduce the side love level in the E-plane, the side love level is still high. Besides, the half power beamwidth (HPBW) at the 5 GHz band is narrow since the width of the proposed antenna is wide. Based on this work, an antenna with better radiation performance will be studied in the next work.

Based on the preceding analysis, the proposed antenna has the advantages of dual-band, compact size, and easy fabrication, which makes it suitable for ceiling mount Wi-Fi access point applications, as shown in Fig. 20.

V. CONCLUSION

In this article, a dual-band MIMO antenna system is investigated. The dual-band microstrip antenna is achieved by exciting the TM_{01} and TM_{03} modes. The resonant frequency of the TM_{01} mode is independently tuned owing to the different electric field intensity distributions of the two modes. The antenna decoupling at the two WLAN bands is realized in a methodological way. The mutual coupling is first reduced at the lower band by independently adjusting the CM and DM impedances. Then, high isolation is obtained at the upper band without affecting the isolation performance at the lower band. The proposed configuration obtains 15.3 dB isolation within the 2.4 and 5 GHz bands.

REFERENCES

[1] M. A. Jensen and J. W. Wallace, "A review of antennas and propagation for MIMO wireless communications," *IEEE Trans. Antennas Propag.*, vol. 52, no. 11, pp. 2810–2824, Nov. 2004.

[2] J. Sui, Y. Dou, X. Mei, and K.-L. Wu, "Self-curing decoupling technique for MIMO antenna arrays in mobile terminals," *IEEE Trans. Antennas Propag.*, vol. 68, no. 2, pp. 838–849, Feb. 2020.

[3] J. Hu, W. Zhang, Y. Li, and Z. Zhang, "Compact co-polarized PIFAs for full-duplex application based on CM/DM cancellation theory," *IEEE Trans. Antennas Propag.*, vol. 69, no. 11, pp. 7103–7110, Nov. 2021.

[4] Y. He and Y. Li, "Compact co-linearly polarized microstrip antenna with fence-strip resonator loading for in-band full-duplex systems," *IEEE Trans. Antennas Propag.*, vol. 69, no. 11, pp. 7125–7133, Nov. 2021.

[5] Y. Li, Z. Zhang, J. Zheng, and Z. Feng, "Compact azimuthal omnidirectional dual-polarized antenna using highly isolated colocated slots," *IEEE Trans. Antennas Propag.*, vol. 60, no. 9, pp. 4037–4045, Sep. 2012.

[6] Y. Li, Z. Zhang, Z. Feng, and M. F. Iskander, "Design of omnidirectional dual-polarized antenna in slender and low-profile column," *IEEE Trans. Antennas Propag.*, vol. 62, no. 4, pp. 2323–2326, Apr. 2014.

[7] Y. Zhang and Y. Li, "Scalable omnidirectional dual-polarized antenna using cavity and slot-dipole hybrid structure," *IEEE Trans. Antennas Propag.*, vol. 70, no. 6, pp. 4215–4223, Jun. 2022.

[8] M. S. Sharawi, S. S. Iqbal, and Y. S. Faouri, "An 800 MHz 2×1 compact MIMO antenna system for LTE handsets," *IEEE Trans. Antennas Propag.*, vol. 59, no. 8, pp. 3128–3131, Aug. 2011.

[9] J. OuYang, F. Yang, and Z. M. Wang, "Reducing mutual coupling of closely spaced microstrip MIMO antennas for WLAN application," *IEEE Antennas Wireless Propag. Lett.*, vol. 10, pp. 310–313, 2011.

[10] Y. F. Cheng, X. Ding, W. Shao, and B. Z. Wang, "Reduction of mutual coupling between patch antennas using a polarization-conversion isolator," *IEEE Antennas Wireless Propag. Lett.*, vol. 16, pp. 1257–1260, 2016.

Authorized licensed use limited to: Tsinghua University. Downloaded on December 18,2023 at 07:49:26 UTC from IEEE Xplore. Restrictions apply.

[11] S. Zhang and G. F. Pedersen, "Mutual coupling reduction for UWB MIMO antennas with a wideband neutralization line," *IEEE Antennas Wireless Propag. Lett.*, vol. 15, pp. 166–169, 2016.

[12] M. Li, B. G. Zhong, and S. W. Cheung, "Isolation enhancement for MIMO patch antennas using near-field resonators as coupling-mode transducers," *IEEE Trans. Antennas Propag.*, vol. 67, no. 2, pp. 755–764, Feb. 2019.

[13] W. Zhang, J. Hu, Y. Li, and Z. Zhang, "Design of a stacked co-polarized full-duplex antenna with broadside radiation," *IEEE Trans. Antennas Propag.*, vol. 69, no. 11, pp. 7111–7118, Nov. 2021.

[14] J. Deng, J. Li, L. Zhao, and L. Guo, "A dual-band inverted-F MIMO antenna with enhanced isolation for WLAN applications," *IEEE Antennas Wireless Propag. Lett.*, vol. 16, pp. 2270–2273, 2017.

[15] S. Nandi and A. Mohan, "A compact dual-band MIMO slot antenna for WLAN applications," *IEEE Antennas Wireless Propag. Lett.*, vol. 16, pp. 2457–2460, 2017.

[16] W. Zhang, Y. Li, K. Wei, and Z. Zhang, "Dual-band decoupling for two back-to-back PIFAs," *IEEE Trans. Antennas Propag.*, vol. 71, no. 3, pp. 2802–2807, Mar. 2023.

[17] Z. Niu, H. Zhang, Q. Chen, and T. Zhong, "Isolation enhancement in closely coupled dual-band MIMO patch antennas," *IEEE Antennas Wireless Propag. Lett.*, vol. 18, no. 8, pp. 1686–1690, Aug. 2019.

[18] F. Liu, J. Guo, L. Zhao, G. Huang, Y. Li, and Y. Yin, "Dual-band metasurface-based decoupling method for two closely packed dual-band antennas," *IEEE Trans. Antennas Propag.*, vol. 68, no. 1, pp. 552–557, Jan. 2020.

[19] X. Tan, W. Wang, Y. Wu, Y. Liu, and A. A. Kishk, "Enhancing isolation in dual-band meander-line multiple antenna by employing split EBG structure," *IEEE Trans. Antennas Propag.*, vol. 67, no. 4, pp. 2769–2774, Apr. 2019.

[20] S. Luo, Y. Li, and W. Shi, "A dual-frequency antenna array with mutual coupling reduction via metamaterial structures," in *Proc. IEEE Int. Symp. Antennas Propag. USNC/URSI Nat. Radio Sci. Meeting*, Jul. 2018, pp. 1385–1386.

[21] H.-L. Peng, R. Tao, W.-Y. Yin, and J.-F. Mao, "A novel compact dual-band antenna array with high isolations realized using the neutralization technique," *IEEE Trans. Antennas Propag.*, vol. 61, no. 4, pp. 1956–1962, Apr. 2013.

[22] B. L. Dhevi, K. S. Vishvaksenan, and K. Rajakani, "Isolation enhancement in dual-band microstrip antenna array using asymmetric loop resonator," *IEEE Antennas Wireless Propag. Lett.*, vol. 17, no. 2, pp. 238–241, Feb. 2018.

[23] J. Xun, L. Shi, W. Liu, G. Liu, and S. Chen, "Compact dual-band decoupling structure for improving mutual coupling of closely placed PIFAs," *IEEE Antennas Wireless Propag. Lett.*, vol. 16, pp. 1985–1989, 2017.

[24] X. Shen et al., "Decoupling of two strongly coupled dual-band antennas with reactively loaded dummy element array," *IEEE Access*, vol. 7, pp. 154672–154682, 2019.

[25] X. Wang and L. Xu, "Coupling reduction in closed coupled dual-band patch antennas," in *Proc. 13th Int. Symp. Antennas, Propag. EM Theory (ISAPE)*, Dec. 2021, pp. 1–3.

[26] J. Sui and K. Wu, "A general T-stub circuit for decoupling of two dual-band antennas," *IEEE Trans. Microw. Theory Techn.*, vol. 65, no. 6, pp. 2111–2121, Jun. 2017.

[27] K. Xu, H. Luyen, and N. Behdad, "A decoupling and matching network design for single- and dual-band two-element antenna arrays," *IEEE Trans. Microw. Theory Techn.*, vol. 68, no. 9, pp. 3986–3999, Sep. 2020.

[28] L. Zhao and K. Wu, "A dual-band coupled resonator decoupling network for two coupled antennas," *IEEE Trans. Antennas Propag.*, vol. 63, no. 7, pp. 2843–2850, Jul. 2015.

[29] M. Li, L. Jiang, and K. L. Yeung, "Applying power dividers to decoupling of MIMO antennas with wideband, dual-band or adjacent-band operations," in *Proc. IEEE Asia–Pacific Microw. Conf. (APMC)*, Dec. 2020, pp. 869–871.

[30] X. Tang, K. Mouthaan, and J. C. Coetzee, "Dual-band ecoupling and matching network design for very closely paced antennas," in *Proc. 42nd Eur. Microw. Conf.*, Oct. 2012, pp. 49–52.

[31] C. Li, X.-Q. Wu, and S. Wang, "A H-shaped dual-band microstrip patch antenna with large frequency ratio under dual modes," in *Proc. IEEE Asia–Pacific Microw. Conf. (APMC)*, Dec. 2020, pp. 822–824.

[32] N.-W. Liu, L. Zhu, and W.-W. Choi, "A differential-fed microstrip patch antenna with bandwidth enhancement under operation of TM_{10} and TM_{30} modes," *IEEE Trans. Antennas Propag.*, vol. 65, no. 4, pp. 1607–1614, Apr. 2017.

[33] L. Sun, Y. Li, Z. Zhang, and H. Wang, "Antenna decoupling by common and differential modes cancellation," *IEEE Trans. Antennas Propag.*, vol. 69, no. 2, pp. 672–682, Feb. 2021.

[34] L. Sun, Y. Li, and Z. Zhang, "Decoupling between extremely closely spaced patch antennas by mode cancellation method," *IEEE Trans. Antennas Propag.*, vol. 69, no. 6, pp. 3074–3083, Jun. 2021.

[35] D. R. Hendry and A. M. Abbosh, "Coupled-resonator theory of isolation in multi-mode antennas," *IEEE Trans. Antennas Propag.*, vol. 67, no. 9, pp. 5801–5811, Sep. 2019.

Weiquan Zhang received the B.S. degree from the University of Electronic Science and Technology of China, Chengdu, China, in 2018. He is currently pursuing the Ph.D. degree in electrical engineering with Tsinghua University, Beijing, China.

His current research interests include reconfigurable antennas, multimode antennas, and reflectarray antennas.

Yue Li (Senior Member, IEEE) received the B.S. degree in telecommunication engineering from Zhejiang University, Hangzhou, Zhejiang, China, in 2007, and the Ph.D. degree in electronic engineering from Tsinghua University, Beijing, China, in 2012.

In June 2012, he was a Post-Doctoral Fellow with the Department of Electronic Engineering, Tsinghua University. In December 2013, he was a Research Scholar with the Department of Electrical and Systems Engineering, University of Pennsylvania, Philadelphia, PA, USA. He was also a Visiting Scholar with the Institute for Infocomm Research (I2R), A∗STAR, Singapore, in 2010, and the Hawaii Center of Advanced Communication (HCAC), University of Hawaii at Manoa, Honolulu, HI, USA, in 2012. Since January 2016, he has been with Tsinghua University, where he is currently an Assistant Professor and an Associate Professor with the Department of Electronic Engineering. He has authored and coauthored over 200 journal articles and 50 international conference papers. He holds 25 granted Chinese patents. His current research interests include metamaterials, plasmonics, electromagnetics, nanocircuits, mobile and handset antennas, multiple-input and multiple-output (MIMO) and diversity antennas, and millimeter-wave antennas, and arrays.

Dr. Li was a recipient of the Issac Koga Gold Medal from URSI General Assembly in 2017, the Second Prize of Science and Technology Award of China Institute of Communications in 2017, the Young Scientist Award from the conferences of Progress in Electromagnetics Research Symposium (PIERS) 2019, International Applied Computational Electromagnetics Society Symposium (ACES) 2018, Atlantic Radio Science Conference (AT-RASC) 2018, Asia-Pacific Radio Science Conference (AP-RASC) 2016, International Symposium on Electromagnetic Theory (EMTS) 2016, and URSI General Assembly and Scientific Symposium (GASS) 2014; the Best Paper Award from the conferences of PhotonIcs & Electromagnetics Research Symposium (PIERS) 2021, International Workshop on Electromagnetics (iWEM) 2021, Asia-Pacific Conference on Antennas and Propagation (APCAP) 2020 and 2017, U.K.-Europe-China Workshop on Millimeter Waves and Terahertz Technologies (UCMMT) 2020, International Symposium on Antennas and Propagation (ISAP) 2019, Cross Strait Quad-Regional Radio Science and Wireless Technology Conference (CSQRWC) 2018, International Symposium on Antennas, Propagation and EM Theory (ISAPE) 2021 and 2016, International Conference on Microwave and Millimeter Wave Technology (ICMMT) 2020 and 2016, National Conference on Microwave and Millimeter Waves (NCMMW) 2018 and 2017, National Conference on Antennas (NCANT) 2019 and 2017; the Outstanding Doctoral Dissertation of Beijing Municipality in 2013, and the Principal Scholarship of Tsinghua University in 2011. He is serving as an Associate Editor for the IEEE TRANSACTIONS ON ANTENNAS AND PROPAGATION, IEEE ANTENNAS AND WIRELESS PROPAGATION LETTERS, Microwave and Optical Technology Letters, and Computer Applications in Engineering Education. He is also serving on the Editorial Board of Scientific Reports Sensors, and Electronics.

Authorized licensed use limited to: Tsinghua University. Downloaded on December 18,2023 at 07:49:26 UTC from IEEE Xplore. Restrictions apply.

Kunpeng Wei (Senior Member, IEEE) received the B.S. degree in electronic and information engineering from the Huazhong University of Science and Technology, Wuhan, China, in 2008 and the Ph.D. degree in electrical engineering from Tsinghua University, Beijing, China, in 2013.

From July 2013 to December 2015, he was with the Radar Research Institute of Chinese Air Force Research Laboratory, Beijing, conducting research in the areas of phased-array antenna design and radar system design. He joined Consume Business Group of Huawei Inc., Xi'an, China, in 2016, where he had been an Antenna Specialist and the Director of Xi'an Antenna Team for five years. In 2021, He joined Honor Device Company Ltd., Beijing, when this company split from Huawei and he was the Director of Honor Antenna Team. After leaving Honor, he joined Xiaomi Corporation, Beijing, in 2023. He is currently the Chief Antenna Expert and the Head of the Antenna Technology Team. He leads a large group of antenna experts and engineers, and takes full responsibility for the research of antenna technologies to guarantee the market success of all Xiaomi's products ranging from smartphones, electric cars, tablets, laptops, and other Internet of Things (IOT) devices. He is a special-level external expert at the China Academy of Information and Communications Technology. And he is also an Adjunct Professor with School of Electronics and information engineering, Shenzhen University, China. He has authored over referred 50 articles on consumer electronics antenna design. He holds over 50 granted U.S./EU/JP/CN patents and has other 20+ patent applications pending. His current research interests include meta-antennas, smart-phone antenna design, small-size 5G antenna systems in terminal devices, and millimeter-wave antenna arrays.

Dr. Wei is an IET Fellow. He was a recipient of the Principal Scholarship of Tsinghua University in 2012, the Huawei Individual Gold Medal Award in 2018, the Huawei Team Gold Medal Award in 2017, and the Honor Team Gold Medal Award in 2021, respectively. He is serving as an Associate Editor of IET Electronics Letters since October 2021.

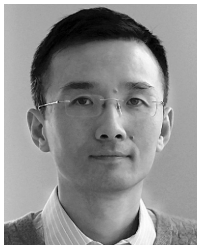

Zhijun Zhang (Fellow, IEEE) received the B.S. and M.S. degrees from the University of Electronic Science and Technology of China, Chengdu, China, in 1992 and 1995, respectively, and the Ph.D. degree from Tsinghua University, Beijing, China, in 1999.

In 1999, he was a Post-Doctoral Fellow with the Department of Electrical Engineering, University of Utah, Salt Lake City, UT, USA, where he was appointed a Research Assistant Professor, in 2001. In May 2002, he was an Assistant Researcher with the University of Hawaii at Manoa, Honolulu, HI, USA. In November 2002, he joined Amphenol T&M Antennas, Vernon Hills, IL, USA, as a Senior Staff Antenna Development Engineer and was then promoted to the position of Antenna Engineer Manager. In 2004, he joined Nokia Inc., San Diego, CA, USA, as a Senior Antenna Design Engineer. In 2006, he joined Apple Inc., Cupertino, CA, as a Senior Antenna Design Engineer and was then promoted to the position of Principal Antenna Engineer. Since August 2007, he has been with Tsinghua University, where he is a Professor in the Department of Electronic Engineering. He is the author of *Antenna Design for Mobile Devices* (Wiley, 1st ed. 2011, 2nd ed. 2017). He served as Associate Editor of the IEEE TRANSACTIONS ON ANTENNAS AND PROPAGATION (2010–2014) and the IEEE ANTENNAS AND WIRELESS PROPAGATION LETTERS (2009–2015).

Authorized licensed use limited to: Tsinghua University. Downloaded on December 18,2023 at 07:49:26 UTC from IEEE Xplore. Restrictions apply.